Component-Wise measure of elastic energy contributions in laminated composite beams

Composite Structures 355 (2025) 118842

Contents lists available at ScienceDirect

Composite Structures

journal homepage: www.elsevier.com/locate/compstruct

Component-Wise measure of elastic energy contributions in laminated composite beams

R. Augello *, E. Carrera, S. Saputo

Mul2 Lab, Department of Mechanical and Aerospace Engineering, Politecnico di Torino, Corso Duca degli Abruzzi 24, 10129 Torino, Italy

ARTICLE INFO

Keywords:
Component-wise
Composites
Carrera Unified Formulation
1D models
Deformation energy

ABSTRACT

This paper investigates the energy distribution in fibre-reinforced composites at the macro-, meso-, and micro-scales. Specifically, the energy contained within the laminate (macro-scale), the layers (meso-scale), and the fibres and matrix (micro-scale) is evaluated. To develop cost-efficient and reliable mathematical models capable of addressing the different scales of the composite structure, one-dimensional (1D) refined finite elements are adopted using the Carrera Unified Formulation (CUF). CUF facilitates the straightforward development of mathematical models at various scales through the use of flexible expansion polynomials, resulting in a three-dimensional (3D) description of the problem using 1D finite elements. The Component-Wise (CW) approach is employed to construct the models at these different scales. Through numerical analysis and comparison with solid finite element models, this study demonstrates that, while the total energy absorbed by a structure under specific loading conditions remains constant, modeling the structure at different scales provides valuable insights into the energy distribution across various components. Additionally, an alternative approach combining the micro- and meso-scales is proposed, in which only one fibre is treated as kinematically independent from the surrounding domains. The results emphasize the accuracy of the different models in capturing the energy distribution, when compared to those obtained from Abaqus analysis using 3D solid elements. Moreover, the proposed technique demonstrates its capability to accurately describe the energy distribution within the composite structure, offering insights into how the structure can withstand external loads and informing design strategies.

1. Introduction

Composite materials offer significant advantages in terms of performance, efficiency, and cost-effectiveness, leading to an increasing use of these structures in various engineering fields, such as aerospace, automotive, and marine industries. Despite the growing adoption of composite materials, several unresolved issues still require further investigation to improve existing design methodologies. In particular, composite structures exhibit various length scales, which are especially evident in fibre-reinforced composites, where the scales include the sub-lamina (fibre and matrix), lamina, and laminate levels. Accurate modeling of these scales and their interactions is important to obtain reliable stress fields and assessing the structural integrity of composite structures.

It is crucial for researchers to effectively manage the size of these models to balance accuracy with computational practicality. In the context of finite element methods, strain energy is a key metric for assessing structural integrity and identifying areas of maximum stress. This is essential for designing safer components and predicting material failure under different loading conditions and scenarios. The fine level of detail provided by the micro-scale model allows for an in-depth understanding of the effects that external loads and boundary conditions have on the various components of the structure, highlighting their structural response, integrity, and the amount of energy they can absorb before eventual collapse [1]. Evaluating strain energy dissipation in a layered structure is essential to better understand its mechanical behavior and predict potential failure modes. Additionally, while evaluating the strain energy absorbed by the structure as a whole may be correct, it may not provide sufficient information about the behavior of individual components within the structure. In such cases, a method that includes a detailed analysis of strain energy at the component level is essential for identifying areas prone to accumulating high levels of strain energy, which are often precursors to structural failure [2]. Establishing these correlations is key to proactively assessing the health and integrity of a structure, enabling early detection and prevention of potential structural failures.

Various methods exist for calculating accurate stress and strain fields within laminated structures. Classic approaches, such as the

* Corresponding author.
E-mail addresses: riccardo.augello@polito.it (R. Augello), erasmo.carrera@polito.it (E. Carrera), salvatore.saputo@polito.it (S. Saputo).

https://doi.org/10.1016/j.compstruct.2025.118842
Received 16 July 2024; Received in revised form 17 October 2024; Accepted 2 January 2025
Available online 17 January 2025

first-order shear deformation theory and more sophisticated higher-order Equivalent Single Layer (ESL) models, are effective for modeling composite structures at the macro scale. In contrast, Layer-Wise (LW) theories [3,4] provide a detailed view of more localized phenomena at the meso scale, accurately representing the distribution of displacement and stress throughout the thickness of the material. Additionally, there are numerous micro-scale theories that address current challenges in composite design, including methods for overcoming issues such as material failure. These include representative volume element (RVE) virtual testing, the variational asymptotic method, and approaches based on energy principles. However, integrating these theories across the macro-, meso-, and micro-scales is a complex task that often necessitates simplifications and assumptions in the mathematical models.

There are several sophisticated techniques for analyzing laminates, including advanced higher-order models [5–7], trigonometric theories [8], zigzag models [9], mixed variational theories [10,11], and layer-wise methods [12]. Although these methods provide accurate macro- and meso-scale stress solutions, they face challenges when dealing with micro-scale phenomena. To cover this gap, multiscale approaches have become essential in the study of damage and failure in composite materials. These approaches combine broad macroscale analysis with detailed micromechanical analysis at the level of individual constituents. Some examples include the Generalized Method of Cells (GMC) [13], the Representative Volume Element (RVE) [14], and the Mechanics of Structure Genome (MSG) [15]. The success of multiscale approaches depends largely on the accuracy of the micromechanical model.

To accurately assess strain energy, it is essential to use a numerical tool capable of evaluating strain energy in fine detail while maintaining low computational requirements. This necessity leads to the adoption of sophisticated structural models such as the Component-Wise (CW) method [16] and advanced 1D hierarchical models for the multiscale analysis of composite structures. The CW method is a modeling approach where different components of a composite are modeled separately yet cohesively, using a unified formulation. Initially developed within the framework of the Carrera Unified Formulation (CUF) described in [17], this methodology was designed for the analysis of composite laminates, including layers, fibres, and matrix materials. It was subsequently extended to the study of multicomponent aircraft structures [18,19], civil structures [20], and more recently, to the assessment of failure parameters in composites [21]. Through the use of CW, LW, and ESL approaches, made possible by CUF methodology, it is possible to evaluate integral quantities such as strain dissipation energy, with particular emphasis on the selection of the integration domain. By dividing the structure into distinct components and analyzing their individual contributions to the overall strain energy, CUF approach provides detailed insights into how energy is distributed and dissipated throughout the structure. This analysis is a critical tool for predicting and preventing structural failure [22], offering valuable insights for making informed decisions during the design, maintenance, and operational phases of engineering projects.

In this work, practical examples are used to highlight the importance of evaluating deformation energy. Initially, the approach is applied to simple cases such as bending, stretching, and torsion of isotropic beams to assess the methodology. This includes the implementation of the shear locking correction using the Mixed Interpolation of Tensorial Components (MITC) technique, which establishes the reliability of the model and successfully validates its results against those obtained from the Abaqus software. The study then advances to the investigation of more complex composite structures, demonstrating how strain energy is distributed across different scales of the structure. Additionally, an application is presented to evaluate the contribution of various components of the strain energy.

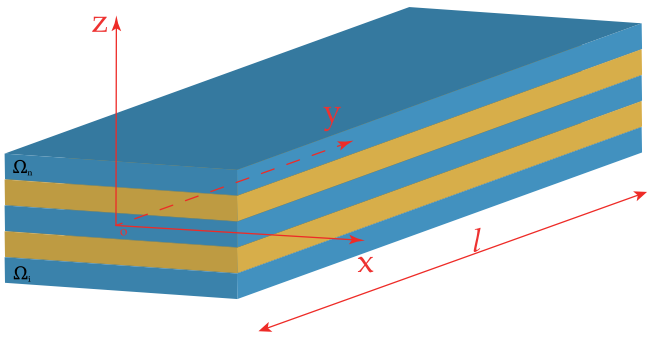

Fig. 1. Generic beam composite structure.

2. Methodology

This section presents the mathematical model and the governing equations used to obtain the results. The motivation for recalling the CUF formalism is explained, as it enables the straightforward development of mathematical models for composite structures without the need for an *ad-hoc* formulation. Specifically:

- Section 2.1 details the refined one-dimensional model employed to describe both metallic and composite structures, providing information on different scales.
- Section 2.2 focuses on the finite element formulation and the derivation of the governing equations, emphasizing the principle of virtual work.
- Section 2.3 explains how the strain energy and its components (both in-plane and out-of-plane) are computed.

2.1. Refined one-dimensional beam model

Consider a composite beam as illustrated in Fig. 1. The coordinate y of a Cartesian reference system lies along the axis direction with length l. The cross-section of the beam in the $x-z$ plane is identified by Ω. The beam section can be determined by summing the subdomains Ω_i, provided they do not overlap.

$$\Omega = \sum_{i=1}^{n} \Omega_i \tag{1}$$

The displacement, strain and stress vectors are expressed in the following:

$$\mathbf{u}(x, y, z) = \{u_x, u_y, u_z\}^T \tag{2}$$

$$\epsilon = \{\epsilon_{xx}, \epsilon_{yy}, \epsilon_{zz}, \epsilon_{xz}, \epsilon_{yz}, \epsilon_{xy}\}^T \; ; \quad \sigma = \{\sigma_{xx}, \sigma_{yy}, \sigma_{zz}, \sigma_{xz}, \sigma_{yz}, \sigma_{xy}\}^T \tag{3}$$

According to linear strain–displacement relations, the strain vector can be written as:

$$\epsilon = \mathbf{D}\mathbf{u} \tag{4}$$

where $\mathbf{D}$ is the differential matrix operator, which explicit form is

$$\mathbf{D} = \begin{bmatrix} \frac{\partial}{\partial x} & 0 & 0 \\ 0 & \frac{\partial}{\partial y} & 0 \\ 0 & 0 & \frac{\partial}{\partial z} \\ \frac{\partial}{\partial z} & 0 & \frac{\partial}{\partial x} \\ 0 & \frac{\partial}{\partial z} & \frac{\partial}{\partial y} \\ \frac{\partial}{\partial y} & \frac{\partial}{\partial x} & 0 \end{bmatrix} \tag{5}$$

The constitutive relation in its linear form is used to relate the stress and the strain as:

$$\boldsymbol{\sigma} = \mathbf{C}\boldsymbol{\epsilon} \tag{6}$$

where $\mathbf{C}$ is material elastic matrix [23,24].

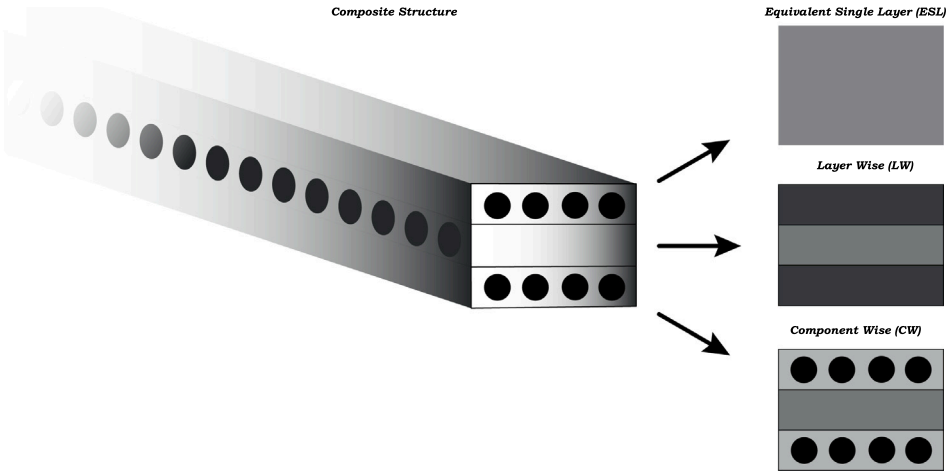

Fig. 2. Composite layered beam and Equivalent Single layer, Layer-Wise and Component Wise approach.

The generalized three-dimensional displacement vector, within the context of the Carrera Unified Formulation (CUF), may be represented as a generic expansion of the primary unknowns, articulated in the following manner:

$$\begin{aligned} \boldsymbol{u}(x,y,z) &= F_\tau(x,z)\,\boldsymbol{u}_\tau(y), \quad \tau = 1,2,\ldots,M \\ \delta\boldsymbol{u}(x,y,z) &= F_s(x,z)\,\delta\boldsymbol{u}_s(y), \quad s = 1,2,\ldots,M \end{aligned} \tag{7}$$

where F_τ and F_s represent the expansion functions corresponding to the generalized displacements $\boldsymbol{u}_\tau$ and the generalized virtual variations $\boldsymbol{\delta u}_s$, respectively. It is assumed that the summing convention is applied with repeated indices τ and s. Finally, M is related to the adopted structural theory.

Macro-, meso-, micro-scale

The various scales at which the composite material beam is represented are displayed in Fig. 2.

- **Equivalent Single Layer (ESL)**: The Equivalent Single Layer (ESL) approach involves merging the properties of the constituents into a single layer. The refinement of the model is dictated by the polynomial order of F_τ and F_s and remains unaffected by the original composite's layer count. In this work, Taylor Expansions (TE) are used for the ESL approach. In ESL models, the continuity of transverse stresses across the laminate and the piecewise discontinuity of displacement derivatives are typically not satisfied.
- **Layer-Wise (LW)**: Layer-Wise (LW) modeling treats each layer independently, utilizing Lagrange-type expansion functions (LE) while ensuring the continuity of transverse stresses through the use of high-order polynomials for beam kinematics. This approach, however, neglects the high stress gradients occurring at the fibre–matrix scale.
- **Component-Wise (CW)**: The Component-Wise (CW) methodology offers flexibility by allowing users to adjust the accuracy of the analysis. This is achieved first by detailing the geometric features of the model (including layers, fibres, and matrices) within a unified formulation, and second, by hierarchically enriching the kinematics through the desired order of LE expansion in specific regions of the structure.

Taylor expansion. Both classic and higher-order theories can be readily derived from Eq. (7) by employing Taylor polynomials of varying orders as F_τ and F_s. This category of polynomials has demonstrated effectiveness in analyzing thin and homogeneous structures [17]. As an example, the generic Taylor expansion of order two for the 1D case is provided below:

$$\begin{aligned} u_x(x,y,x) &= u_{x_1} + u_{x_2}x + u_{x_3}z + u_{x_4}xz + u_{x_5}z^2 \\ u_y(x,y,x) &= u_{y_1} + u_{y_2}x + u_{y_3}z + u_{y_4}xz + u_{y_5}z^2 \\ u_z(x,y,x) &= u_{z_1} + u_{z_2}x + u_{z_3}z + u_{z_4}xz + u_{z_5}z^2 \end{aligned} \tag{8}$$

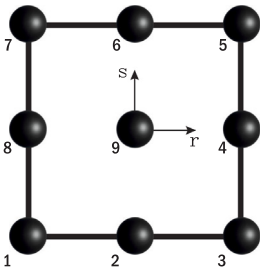

Fig. 3. Schematic representation of element with nine Lagrange points designed specifically for beams.

Lagrange expansion. In this case, the cross-section is approximated with a pattern of Lagrange Points (LPs), which are divided into appropriate Lagrange polynomials. The 3D displacement field is then a result of an interpolation of the displacements calculated at the LPs. The degree of the interpolation is defined by the number of employed LPs. For instance, if a quadratic interpolation is employed, the interpolation functions for the 1D beam models are:

$$\begin{aligned} F_\tau &= \frac{1}{4}\left(r^2 + rr_\tau\right)\left(s^2 + ss_\tau\right) && \tau = 1,3,5,7 \\ F_\tau &= \frac{1}{2}s_\tau^2\left(s^2 - ss_\tau\right)\left(1 - r^2\right) + \frac{1}{2}r_\tau^2\left(r^2 - rr_\tau\right)\left(1 - s^2\right) && \tau = 2,4,6,8 \\ F_\tau &= \left(1 - r^2\right)\left(1 - s^2\right) && \tau = 9 \end{aligned} \tag{9}$$

where r and s are the natural coordinates from −1 to +1 of a generic point on the cross-section, and r_τ and s_τ are the natural coordinates of the nine LPs, as shown in Fig. 3. Readers are referred to [17] for the mathematical steps to transform the natural coordinates into physical ones.

2.2. Governing equations

The generalized displacement $\mathbf{u}_\tau$ and its variation $\mathbf{u}_s$ introduced in the Eq. (7) can be discetized employing the Finite Element Method (FEM) as:

$$\mathbf{u}_\tau(y) = N_i(y)\,\mathbf{q}_{\tau i} i = 1,2,\ldots,N_n$$

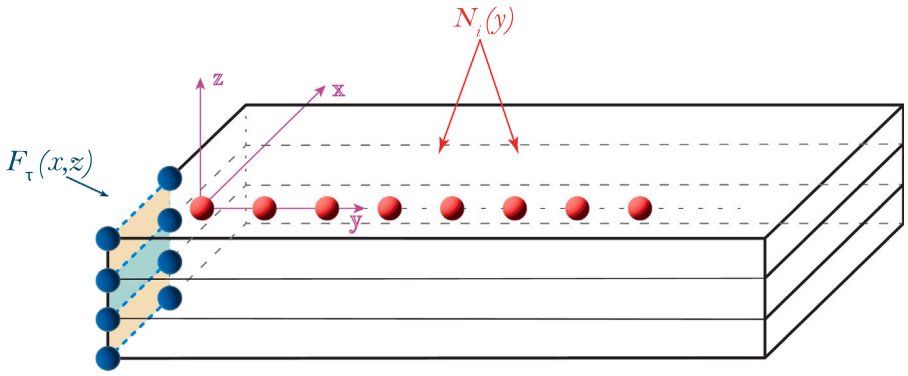

Fig. 4. Mathematical models of the 1D beam.

$$\delta \mathbf{u}_s(y) = N_j(y)\,\delta \mathbf{q}_{si} j = 1, 2, \ldots, N_n \tag{10}$$

where N_i and N_j represent the shape functions, and the repeated subscripts i and j indicate summation. N_n denotes the number of Finite Element (FE) nodes per element, while the vectors representing the nodal parameters are respectively $\boldsymbol{q}_{\tau i}$ and $\boldsymbol{q}_{sj}$. A schematic representation can be observed in Fig. 4

$$\begin{aligned} \mathbf{q}_{\tau i} &= \left\{ q_{x_{\tau i}} \quad q_{y_{\tau i}} \quad q_{z_{\tau i}} \right\}^T \\ \mathbf{q}_{sj} &= \left\{ q_{x_{sj}} \quad q_{y_{sj}} \quad q_{z_{sj}} \right\}^T \end{aligned} \tag{11}$$

The governing equations are deduced from the principle of virtual displacements (PVD). For elastic bodies in a state of static equilibrium, the following relationship holds:

$$\delta L_{\text{int}} = \delta L_{\text{ext}} \tag{12}$$

where with δL_{int} is expressed the strain energy variation due to deformations and δL_{ext} stands the work done by external forces on virtual displacements. The variation in internal energy δL_{int} can be expressed as:

$$\delta L_{\text{int}} = \int_V \delta \varepsilon^T \boldsymbol{\sigma}\, dV \tag{13}$$

By employing the displacement functions, geometric relations, and constitutive equations, Eq. (13) is rewritten as:

$$\begin{aligned} \delta L_{int} &= \delta \boldsymbol{u}_{js}^T \int_V N_j \mathbf{I} F_s \boldsymbol{D}^T \boldsymbol{C} \boldsymbol{D} F_\tau \mathbf{I} N_i dV \boldsymbol{u}_{i\tau} \\ &= \delta \mathbf{q}_{js}^T \mathbf{k}^{ij\tau s} \mathbf{q}_{i\tau} \end{aligned} \tag{14}$$

Where $\mathbf{k}^{ij\tau s}$ is a 3×3 matrix, called the Fundamental Nucleus (FN) of the mechanical stiffness matrix. The nucleus serves as the basic element from which the stiffness matrix of the entire structure is computed. The fundamental nucleus is expanded across indices i and j to obtain the stiffness matrix.

The virtual work δL_{ext} carried out by the external load p is given by:

$$\delta L_{\text{ext}} = \int_V \delta \boldsymbol{u}^T \mathbf{p}\, dV \tag{15}$$

This equation can be further expanded in the CUF form as:

$$\begin{aligned} \delta L_{\text{ext}} &= \delta \mathbf{q}_{js}^T \int_V N_j \mathbf{I} F_s^j \mathbf{p}\, dV \\ &= \delta \mathbf{q}_{js}^T \mathbf{p}_{js} \end{aligned} \tag{16}$$

where $\mathbf{p}_{js}$ is the 3×1 FN of the load vector. By the combination of Eq. (14) and (16) it is possible to write:

$$\delta \mathbf{q}_{js}^T \mathbf{k}^{ij\tau s} \mathbf{q}_{i\tau} = \delta \mathbf{q}_{js}^T \mathbf{p}_{js} \tag{17}$$

The global stiffness matrix is obtained by the summation over the indices i, j, τ, s following the CUF assembling procedure which interested readers can find in [17].

2.3. Strain energy measure through integral expression

To identify the strain dissipation energy locations within composite structures is essential to assess integral quantities within sub-domains, which can be represented as lines, areas, or volumes encompassing components or interfaces between laminae/fibre–matrix layers. This study focuses on evaluating integral quantities such as strain energy in both global and local regions of the structure. In the following each independent subdomains of the structure are denoted as V_i. The strain energy in V_i can be computed as follows:

$$\begin{aligned} E_i &= \int_{V_i} \boldsymbol{\sigma}^T \epsilon\, dV_i \\ E_{ip} &= \int_{V_i} \boldsymbol{\sigma}_n \epsilon_n\, dV_i \qquad n = xx, yy, xy \\ E_{op} &= \int_{V_i} \boldsymbol{\sigma}_m \epsilon_m\, dV_i \qquad m = zz, xz, yz \end{aligned} \tag{18}$$

where E_i, E_{ip}, E_{op} are respectively the total strain energy, the in-plane strain energy and out-of-plane strain energy contributions.

3. Numerical results

In this section, we consider two beam structures made of isotropic and composite materials, bending and torsion loads are applied.

3.1. Metallic beam

The beam is made of Al-7075 aluminum, has a length of 1 m and a cross-sectional area of 0.02 by 0.02 m^2. The root of the beam placed at a height $y = 0$ is considered fixed, while the external load is applied at the end of the beam and shown in Fig. 5.

The finite element model was developed by considering different elements along the beam axis and using various shape functions (linear B2, quadratic B3, and cubic B4). For the cross-section, a nine-point Lagrange element was employed. Additionally, in this phase, various kinematic theories, such as the Timoshenko and Euler–brenoulli beam models, were considered. These are denoted as LE for the Lagrangian model, EB for Euler–brenoulli, and TM for Timoshenko.

Bending

The bending load is included by applying transverse force (along the z-axis) equal to 500 N and applied in center of the section, as shown in Fig. 5(a). Convergence studies on the tip transverse displacement and the total deformation energy are conducted and results are shown in Figs. 6 and Fig. 7, respectively. The values have been compared to a reference value calculated using a refined model which makes use of 80 B4 elements, so that for example $\bar{u}_z = u_z / u_{z_{Ref}}$. Clearly, from both figures it is evident that the use of linear shape functions shown how, with increasing the number of elements, the result tends to converge towards the reference value. However, it appears that the number of

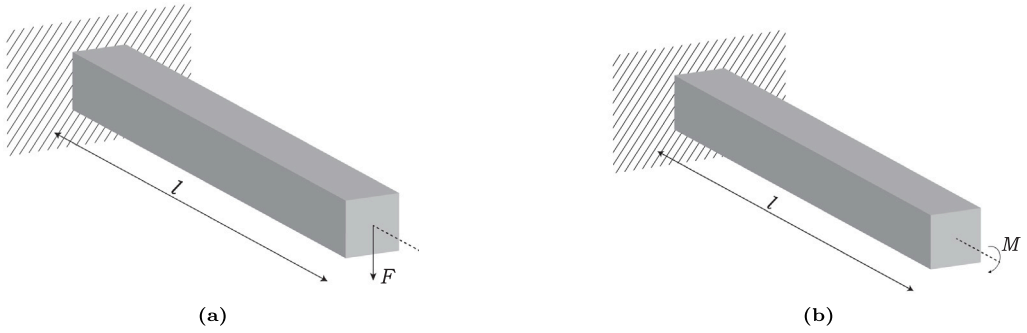

Fig. 5. Load condition for metallic beam, (a) bending case; (b) twisting case.

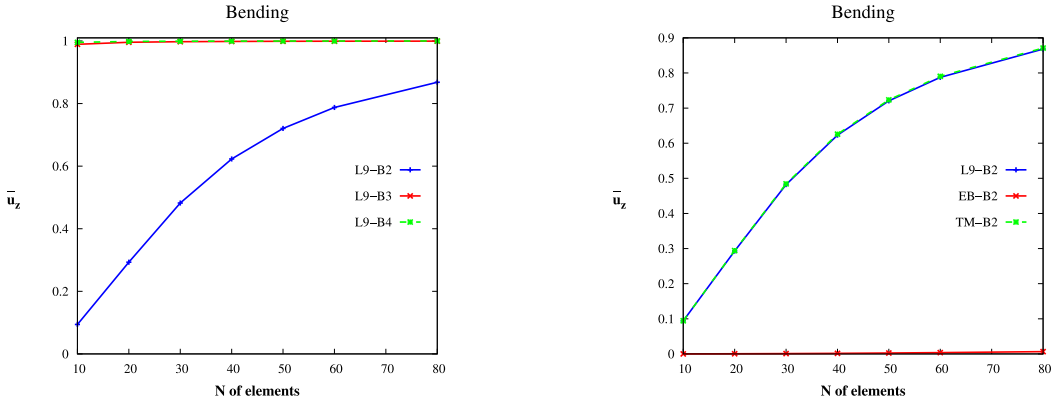

Fig. 6. Bending case: Dimensionless vertical displacement vs number of element.

Table 1
Vertical displacement $\mathbf{u}_z$ [m].

N of Elements							
	10	20	30	40	50	60	80
L9 - B2	−0.016781	−0.052256	−0.085966	−0.111081	−0.128476	−0.140436	−0.154784
EBBT - B2	−0.000019	−0.000074	−0.000167	−0.000297	−0.000463	−0.000666	−0.001181
TMBT - B2	−0.016826	−0.052475	−0.086357	−0.111569	−0.129002	−0.140967	−0.155287
L9 - B3	−0.176417	−0.177596	−0.177923	−0.178068	−0.178147	−0.178196	−0.178250
EBBT - B3	−0.178125	−0.178460	−0.178522	−0.178544	−0.178554	−0.178560	−0.178564
TMBT - B3	−0.178324	−0.178582	−0.178609	−0.178615	−0.178617	−0.178617	−0.178618
L9 - B4	−0.177546	−0.178044	−0.178185	−0.178244	−0.178275	−0.178292	−0.178308
EBBT - B4	−0.178571	−0.178572	−0.178571	−0.178571	−0.178571	−0.178571	−0.178570
TMBT - B4	−0.178618	−0.178618	−0.178618	−0.178618	−0.178618	−0.178618	−0.178618

elements used may not yet be sufficient to accurately describe the bending behavior of the beam. On the other hand, the use of quadratic and cubic shape functions allows reaching the reference value even with a low number of elements. Furthermore, with the same shape functions, the Timoshenko kinematic model provides a displacement field trend that overlaps with the Lagrangian model. Finally, the Euler–brenoulli kinematic model does not exhibit a converging trend towards the reference value.

Additionally, in Table 1, the maximum displacements achieved for the different theories are reported.

In Fig. 7, the trends of the absorbed strain energy are shown, both by varying the shape functions and the number of elements, and by varying only the kinematic models. The same considerations made for the displacement trend can be applied to the energy absorption.

In the case of very thin structures subjected to bending or shear loads, numerical phenomena such as shear locking may occur. To overcome this issue, one approach is to use higher-order elements, which are able to more accurately capture the stress and strain distribution in such cases. Another method is to apply correction techniques, such as the MITC (Mixed Interpolation of Tensorial Components) [25,26] correction factor. MITC is a technique that adjusts the interpolation functions used in finite element formulations to better account for shear deformations, thereby reducing shear locking. This correction factor is particularly effective in improving the accuracy of element formulations under shear-dominated loading conditions. In Fig. 8, it is shown how the application of the correction factor to Euler–brenoulli and Timoshenko structural models significantly improves mechanical behavior in terms of vertical displacement. It can be observed that, even with a reduced number of elements along the beam axis and with linear shape functions, convergence to the reference value is easily achieved. Similar improvements are observed in the trend of energy absorbed by the structure. As in the previous case, the use of a correction factor to mitigate shear locking effects results in a remarkable improvement in the structure's response in terms of absorbed energy.

Table 2 presents the related values of the tip displacement.

Twisting

The applied torsional moment is 9 Nm, applied at the free end of the beam as depicted in Fig. 5(b). As in the previous case, convergence analyses are carried out for the angle of twist and total deformation

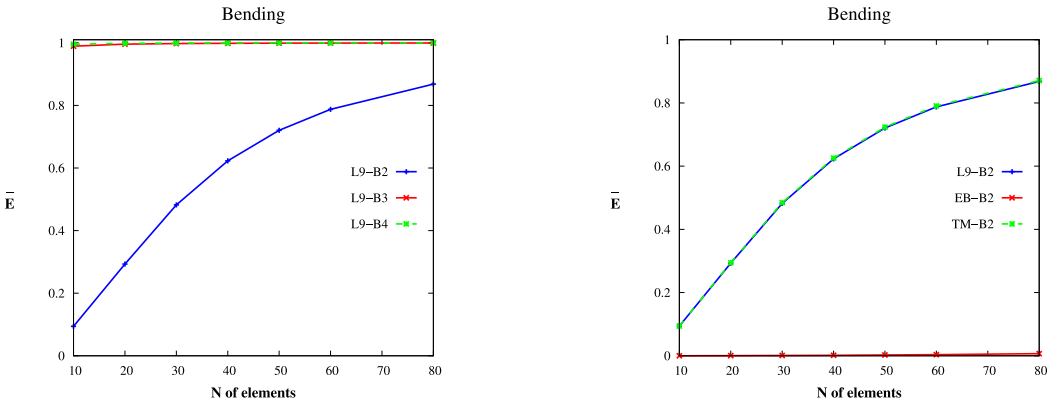

Fig. 7. Bending case: Dimensionless energy vs number of element.

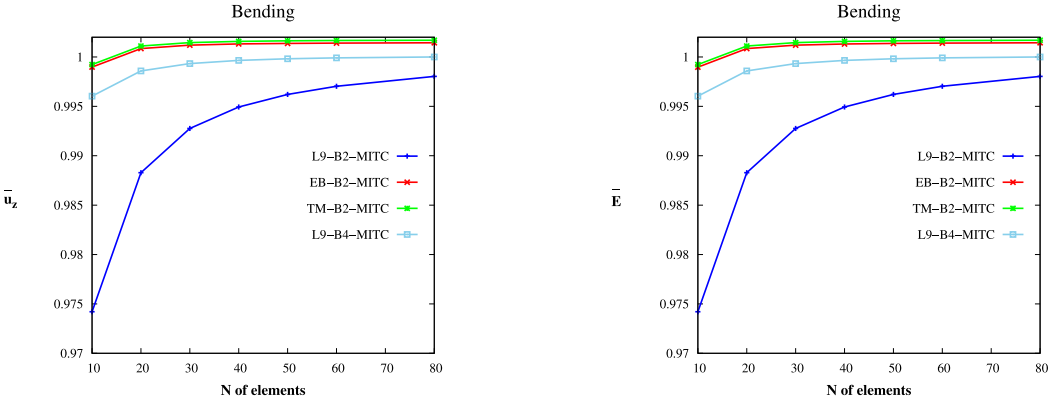

Fig. 8. Bending case: MITC correction factor.

Table 2
Vertical displacement u_z [m] for different adopted theories with MITC.

N of Elements	L9 - B2 MITC	EBBT - B2 MITC	TMBT - B2 MITC	L9 - B4 MITC
10	−0.17370880	−0.17812505	−0.17817143	−0.17760104
20	−0.17621981	−0.17845987	−0.17850625	−0.17805603
30	−0.17701811	−0.17852185	−0.17856825	−0.17818939
40	−0.17740594	−0.17854357	−0.17858996	−0.17824660
50	−0.17763274	−0.17855363	−0.17860000	−0.17827578
60	−0.17778015	−0.17855909	−0.17860546	−0.17829222
80	−0.17795770	−0.17856449	−0.17861088	−0.17830835

energy, shown in Figs. 9 and 10, respectively. The case of torsion shown in Fig. 9(a) highlights an increasing convergence rate with the refinement of the shape function. In particular, the trend for linear elements shows an almost linear behavior, unlike that of quadratic and cubic elements. The behavior exhibited by the beam under torsion, similar to the case of bending, emphasizes an incorrect kinematic response in the case of EB and TM kinematic models, as highlighted in Fig. 9(b).

The energy values shown in Fig. 10(b) exhibit the same trend as the angle. Under torsional loading conditions, the shape functions allow for a significant improvement in kinematic behavior and consequently in the absorbed energy values. On the other hand, the kinematic models of the EB and TM beams fail to reach the reference value even with a high number of elements.

3.2. Composite beam

In this section a composite beam with a stacking sequence of [0/90/0] and a length of 40 mm is introduced. The height of the beam, h, is 0.6 mm and the width, b, is 0.8 mm. Four mathematical models were developed for such structure by means of the CW approach. They are:

- **Model 0 ESL** The whole stacking sequence is homogenized into a single layer, as in the standard ESl approach. Macro-scale degree of accuracy is achieved. (Fig. 11(a))
- **Model 1 LW** The level of detail is meso-scale; the top and bottom layers are considered homogeneous but with a 90-degree variation in material orientation. The modeling approach is LW (Layer Wise). (Fig. 11(b))
- **Model 2 CW** Represents the most refined model presented in this work, where the CW approach is used to kinematically define each fibre. Micro-scale approach. (Fig. 11(c))
- **Model 3 LW-CW** Finally, the third model (LW-CW) 11(d) offers a combination of micro- and meso-scale. In particular, in the lower lamina, a single fibre is discretized using the CW approach (micro-scale), whereas LW is adopted elsewhere (meso-scale) (Fig. 11(d)).

The finite elements along the beam axis adopts cubic shape functions. Some detailed information about the geometry can be found in [27]

We assume the fibre material possesses transverse anisotropy, meaning its material properties are directionally dependent only in the plane

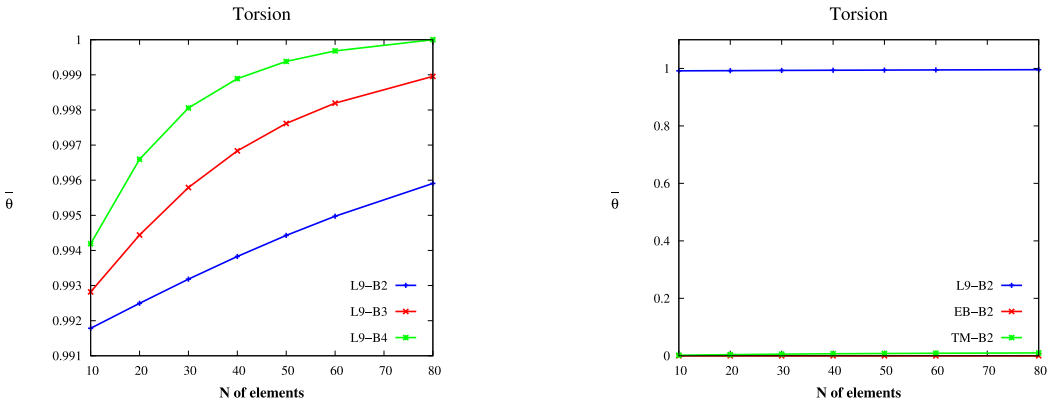

(a) Increasing the shape function. (b) Different expansion function.

Fig. 9. Twisting case: Dimensionless angle vs number of element.

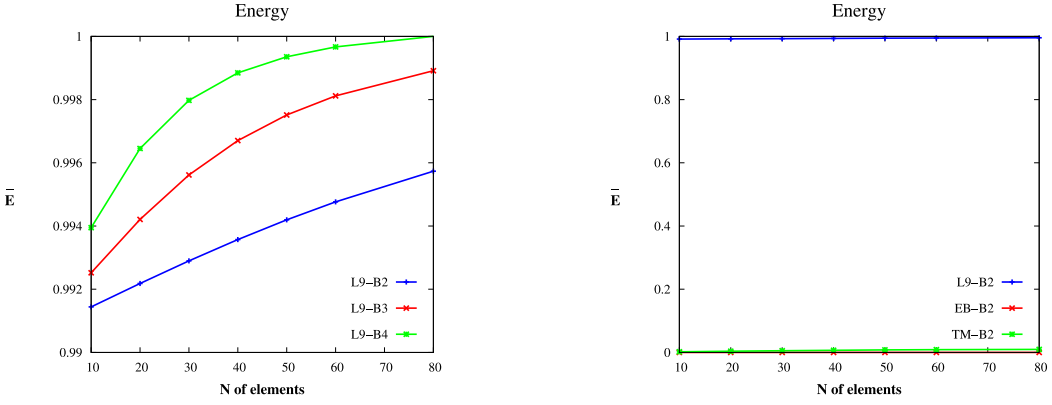

(a) Increasing the shape function. (b) Different expansion function.

Fig. 10. Twisting case: Dimensionless energy absorbed vs number of element.

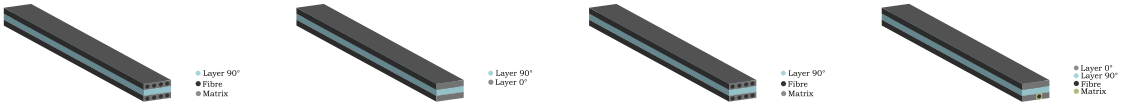

(a) Model 0 ESL (b) Model 1 LW (c) Model 2 CW (d) Model 3 LW-CW

Fig. 11. 0/90/0 modeling strategies.

Table 3
Material properties.

Material properties									
	E_1 [GPa]	E_2 [GPa]	E_3 [GPa]	ν_{12}	ν_{23}	ν_{13}	G_{12} [GPa]	G_{13} [GPa]	$G23_{23}$ [GPa]
Fibre	202.038	12.134	12.134	8.358	8.358	47.756	0.2128	0.2128	0.2704
Layer	103.173	5.145	5.145	2.107	2.107	2.353	0.2835	0.2835	0.3124
Matrix		3.252			0.355			1.2	

perpendicular to the fibre axis. In contrast, the matrix exhibits isotropy, implying its properties are independent of direction. The equivalent layer's engineering constants are subsequently calculated using the established hybrid rules of mixtures approach (Table 3).

Bending. For the bending case, the beam is clamped at one end, while a force of 1 N is applied to the other end at the center of the cross-section. Moreover, to compare the proposed approach with commercial finite element software, a second-order 3D element model with equivalent geometric and physical characteristics to those described for model 2 was created in Abaqus. The Abaqus model was discretized with 320 divisions along the beam axis, compared to the 40 elements used for the CUF approach (for all models). Table 4 presents the results obtained for the various models under consideration and compares them with the Abaqus 3D model. In particular, the stress values are calculated at the point with coordinates l/2, h/6, b/8, while the displacement values are evaluated at the point with coordinates l, h/2, b/2. Finally, the values of strain energy (for the entire beam) and the number of degrees of freedom for the models are reported.

Table 4
Displacement and Stresses of composite beam for different CW and 3D model.

	Abaqus	Model 2	Model 0	Model 1	Model 3
$u_z \times 10^4$ m	−15.53	−15.527	−15.468	−14.91	−14.95
$\sigma_{yy} \times 10^{-6}$ Pa	−5.8597	−5.86478	−5.8488	−2.87962	−5.66517
$\sigma_{yz} \times 10^{-8}$ Pa	−2.2523	−2.5598	−5.7719	−1.67354	−2.81767
Total Energy 10^{-3} J	7.7653	7.7633	7.7342	7.4580	7.4973
Dof	4 932 459	313 995	5445	22 869	59 169

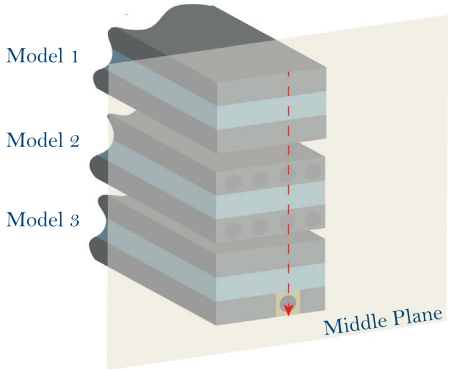

Fig. 12. Path cut for stress trend.

The point values of the stress, for all models, converge with good approximation to the value obtained from the Abaqus model except for model 1.

Subsequently, to understand in detail the stress trend, in accordance with Fig. 12, the stresses were evaluated along the path represented by the dashed red line. As highlighted by the described figure, the path, evaluated along the middle axis of the beam, crosses two fibres in the case of model 0 and 2 and the single fibre present in model 3.

The results are shown in Fig. 13. The component-wise approach (Model 2 and the 3D Abaqus model) reveals that the most critical area for shear stress is at the interface between the bottom region of the matrix and the top region of the fibre. By comparing the shear stress trends, σ_{yy} and σ_{yz}, obtained from the CW model and the Abaqus 3D model, a perfect overlap between the two models is observed, both in terms of trend and values. In contrast, although the LW model exhibits a trend very similar to the reference, it underestimates the stress values and is unable to reach the same point values. However, the LW-CW model underscores the importance of the CW model. Due to the symmetry of the beam with respect to its mid-plane and the applied load, the asymmetry in the results highlights the necessity of a CW model to achieve more accurate results. The stress trend σ_{yy} depicted in Fig. 13(a) demonstrates how Model 0 can predict stress patterns comparable to more sophisticated models, such as Model 2 and the reference Abaqus model. However, the stress trend for σ_{yz}, shown in Fig. 13(b) does not include results for Model 0. This omission is due to the fact that the reference values are overestimated compared to the results of the other models. Including these values in the same graph would obscure clarity. It is also worth noting that this discrepancy in results is well-documented and emphasized in [28].

Even though the values obtained from the four numerical models are approximately the same, the energy distribution in the beam's cross-section differs, as does the amount of energy absorbed by the various components of the beam. The variation in energy absorption among the four models is presented in Table 5.

Il testo è chiaro, ma ci sono alcuni piccoli miglioramenti che possono essere apportati per renderlo più preciso e scorrevole. Ecco una versione rivista:

This table illustrates the trend in energy absorption for model 1 across its three layers, for model 0 and model 2 focusing solely on fibre absorption, and for model 3 considering absorption by the fibres, matrix, and layers. Specifically, in the CW model, fibre absorption is enumerated clockwise from left to right across the beam section, whereas in the LW-CW approach, the fibres in layer 3 are reported last, with the exception of the matrix and fibre discretization. Given the loading conditions and resulting beam deformation, the contribution to energy absorption from layers or matrices perpendicular to the beam axis is negligible compared to the energy absorbed by the fibres. The strain energy distribution over the cross-section for models 1, 2, and 3 is shown in Fig. 14.

Given the physics of the problem, most of the strain energy is concentrated along the top and bottom edges of the cross-section. This distribution is accurately captured by Model 1. In addition, using a micro-scale approach (model 2) allows for examining the energy distribution between different components, and shows that the deformation energy is predominantly concentrated within the fibres, particularly in the sub-volume near the top and bottom of the beam. An intermediate trend is observed in model 3, where the considerations made for models 1 and 2 remain valid. The deformation energy distribution for the models introduced in this study is depicted of Fig. 15. The graph illustrates the overall contributions, including sub-components representing the three layers of the beam. On the left side of the diagram, the energy absorption for the top layer is evident, while the central part illustrates the 90°-oriented layer, and the right side represents the bottom layer.

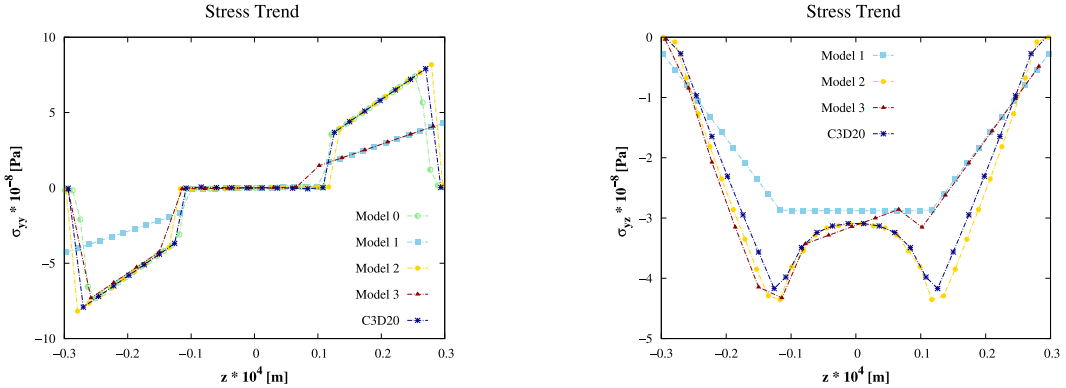

(a) σ_{yy} (b) σ_{yz}

Fig. 13. Axial and shear stress along the thickness.

Table 5
Energy distribution for LW model, Cw model, LW-CW model.

	Energy Distribution							
	Model 0 x 10-3 [J]							
Energy					7.7342			
	Model 1 x 10-3 [J]							
	Layer 0°				Layer 90°			Layer 0°
Energy	3.714				0.0302			3.714
	Model 2 x 10-3 [J] CW							
	Fibre 1	**Fibre 2**	**Fibre 3**	**Fibre 4**	**Fibre 5**	**Fibre 6**	**Fibre 7**	**Fibre 8**
Energy	0.9526	0.9526	0.9526	0.9526	0.9526	0.9526	0.9526	0.9526
	Matrix 1	**Matrix 2**	**Matrix 3**	**Matrix 4**	**Matrix 5**	**Matrix 6**	**Matrix 7**	**Matrix 8**
Energy	0.0178	0.0178	0.017	0.0178	0.0178	0.0178	0.0178	0.0178
	Mode 3 x 10-3 [J]							
	Layer 0°		**Layer 90°**		**Layer 90°**		**Fibre**	**Matrix**
Energy	3.752		0.0310		2.8221		0.8831	0.0774

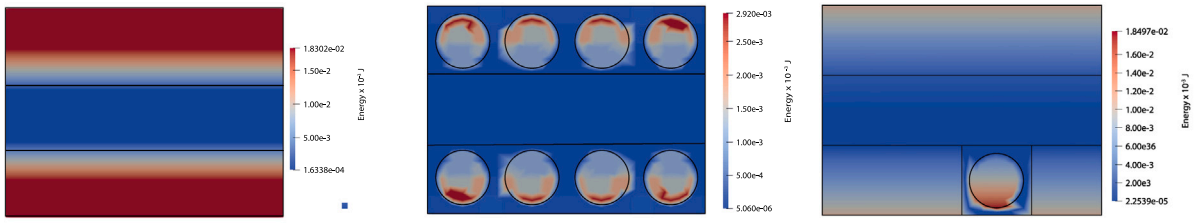

(a) Model 1 LW (b) Model 2 CW (c) Model 3 LW-CW

Fig. 14. Strain dissipation energy for a section slice.

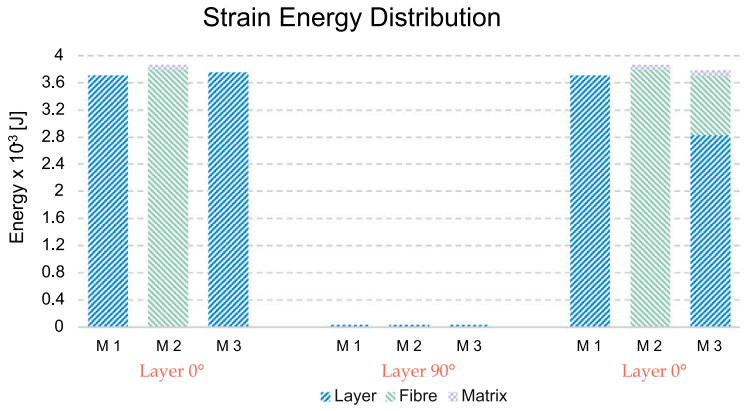

Fig. 15. From left to right, the values of the absorbed deformation energy are reported for the models built with different scales for the top, middle, and bottom layers. The letter "M" refers to the model.

Twisting. In this subsection, the case of a twisting load is considered. The adopted discretization, as well as the mechanical and geometric characteristics of the structure and the approaches at different levels of detail, are the same as in the previous case. The torsional load is applied by introducing two opposing forces at [b/2, ± h/2,L] with a magnitude of 5 N. The choice of modeling scale does not significantly influence the structural response of the beam, as evidenced by the displacement along the x-axis (at the load application point) reported in Table 6 and evaluated at the section where the load is applied. However, a larger variation can be observed both in the point value of the stress (evaluated at the point with coordinates b/8; −h/3; L/2) and in the energy value evaluated by the four proposed discretizations. By illustrating the shear stress distributions in the yz and xy planes as a function of beam thickness, as depicted in Figs. 16(a) and 16(b) respectively, it becomes evident that the discontinuities in these distributions manifest near the fibre–matrix interfaces and between layers.

Table 6
Deformation, stresses and total strain energy of composite beam for different scale under shear load.

	Model 2	Model 0	Model 1	Model 3
$u_z \times 10^4$ m	4.7994	2.1882	5.5452	5.7026
$\sigma_{xy} \times 10^{-7}$ Pa	−0.3260	−0.5695	−1.2253	−0.5750
$\sigma_{yz} \times 10^{-6}$ Pa	6.6769	1.3929	5.6046	7.0162
Total Energy 10^{-3} J	2.3996	1.0941	2.7720	2.7888
Dof	313 995	5445	22 869	59 169

Clearly, accurately capturing the discontinuity between the fibre and the matrix necessitates the use of the CW approach or the LW-CW approach. In contrast, an LW approach only allows for partial identification of shear stress discontinuities between layers.

Let us consider a slice of the beam positioned at L/2, and let us analyze the distribution of strain energy due to the stress conditions in-plane and out-of-plane, respectively depicted in Figs. 17 and 18.

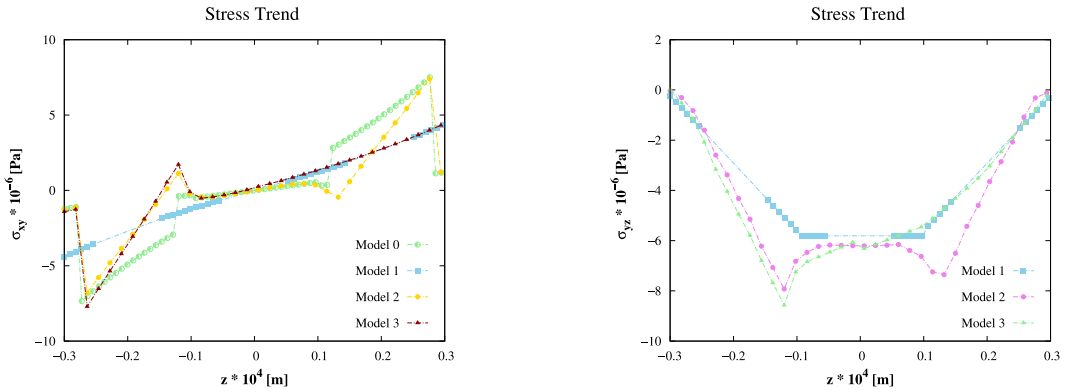

(a) σ_{yy} (b) σ_{yz}

Fig. 16. Shear stresses along the thickness.

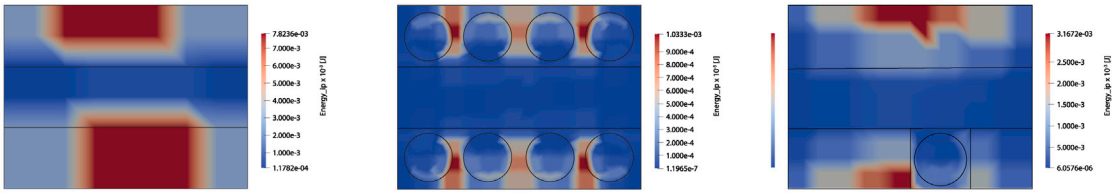

(a) Model 1 LW (In-plane) (b) Model 2 CW (In-plane) (c) Model 3 LW-CW (In-plane)

Fig. 17. In plane deformation energy of a cross-section for the twisting load case.

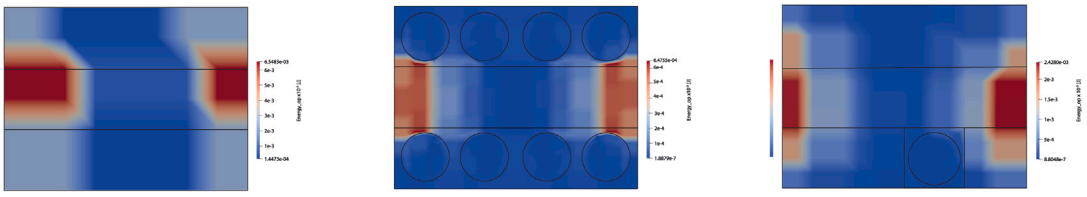

(a) Model 1 LW (Out-plane) (b) Model 2 CW (Out-plane) (c) Model 3 LW-CW (Out-plane)

Fig. 18. Out plane Strain dissipation energy for a section slice for twisting load case.

Model 1 (Fig. 17(a)) concentrates the absorption of in-plane strain energy in the central region of the top and bottom plies, consistent with the physics of the problem. The CW approach (Fig. 17(b)) shows that, under torsional loading, the most stressed area is the interface between the fibre and the matrix. In contrast, in Model 3 (Fig. 17(c)), the absence of the matrix and the presence of only the fibre lead to a redistribution of the energy in a hybrid manner between the LW and CW models.

Fig. 18 shows the distribution over the cross-section of the out of plane component of the deformation energy. The LW model (Fig. 18(a)) reveals a concentration of strain energy in the central layer (0° layer), particularly at the edges of the cross-section. The CW (Fig. 18(b)) like the previous one, highlights that the critical zone for the composite is primarily the interfaces between the various layers, rather than the fibre–matrix interface. In fact, the CW approach shows a peak in energy due to shear stresses precisely at the interface between the outer fibres and the matrix, as well as in the 90° oriented layer. Finally, the LW-CW model (Fig. 18(c)) demonstrates that the presence of a detailed model adjacent to the vertical symmetry plane of the structure does not significantly affect the absorption of out-of-plane strain energy under torsional loading.

The choice to model a sub-volume of a particular layer, as in model 3, affects the strain energy absorption under torsional loading. In the case of Fig. 17(c), the presence of a fibre at a particular position generates a peak of in-plane energy near the fibre itself. Conversely, in Fig. 18(c), a fibre near the vertical symmetry plane of the beam does not affect the out-of-plane energy distribution. To assess the influence of the positioning of a single fibre in the model, we can consider moving the fibre to the edge of the beam cross-section. In this scenario, the energy due to in-plane stresses (Fig. 19(a)) is influenced by the CW model of the fibre, similar to the out-of-plane energy as shown in Fig. 19(b). The spatial arrangement of individual fibres within the composite structure plays a critical role in determining its mechanical response under different loading conditions.

Finally, Table 7 shows the absorbed energy for different assumed scales, divided into in-plane and out-of-plane energy, as well as the total energy. The CUF methodology allows us to evaluate any quantity of interest by integrating it over the volume. By leveraging this feature with a CW approach, it is possible to calculate the strain energy due to individual stress and strain components for the volume of interest. Table 8 summarizes how, in model 2, under bending followed by torsional loading, it is possible to evaluate the portion of strain energy attributable to the six stress and strain components for both the fibre and matrix, which constitute the top and bottom layers. Detailed results of this kind provide valuable insights into the mechanical behavior of composite structures and potential fracture modes.

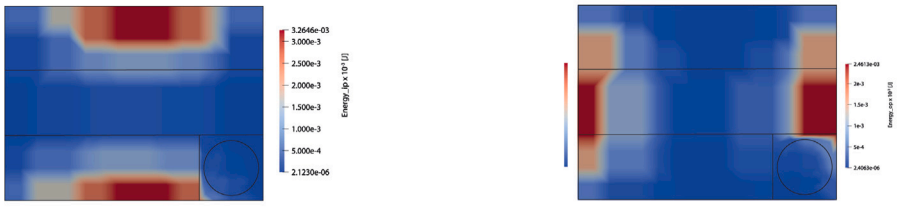

(a) In plane Strain Energy (b) Out-plane Strain Energy

Fig. 19. Strain dissipation energy for a section slice for twisting load case replacing the fibre of model 3.

Table 7
Total energy, bending energy and shear energy distribution for ESL model, LW model, CW model, LW-CW model.

	Energy Distribution							
	Model 0 x 10 $^{-3}$ [J]							
$Energy_{Total}$					1.0941			
$Energy_{Inplane}$					0.7217			
$Energy_{Outplane}$					0.3724			
	Model 1 x 10 $^{-3}$ [J]							
	Layer 0°				**Layer 90°**			**Layer 0°**
$Energy_{Total}$	1.0792				0.6141			1.0792
$Energy_{Inplane}$	0.8571				0.0466			0.8571
$Energy_{Outplane}$	0.2222				0.5675			0.2222
	Model 2 x 10 $^{-3}$ [J]							
	Fibre 1	**Fibre 2**	**Fibre 3**	**Fibre 4**	**Fibre 5**	**Fibre 6**	**Fibre 7**	**Fibre 8**
$Energy_{Total}$	0.0459	0.0845	0.0845	0.0459	0.0658	0.0845	0.0845	0.0459
$Energy_{Inplane}$	0.0384	0.0796	0.0796	0.0385	0.0367	0.0796	0.0796	0.0385
$Energy_{Outplane}$	0.0075	0.0049	0.0049	0.0075	0.0292	0.0049	0.0049	0.0075
	Matrix 1	**Matrix 2**	**Matrix 3**	**Matrix 4**	**Matrix 5**	**Matrix 6**	**Matrix 7**	**Matrix 8**
$Energy_{Total}$	0.1250	0.2089	0.2089	0.125	0.125	0.2089	0.2089	0.125
$Energy_{Inplane}$	0.0635	0.1774	0.0635	0.0635	0.0635	0.1774	0.1774	0.0635
$Energy_{Outplane}$	0.0614	0.0315	0.0315	0.0614	0.0614	0.0315	0.0315	0.0614
	Model 3 x 10 $^{-3}$ [J]							
	Layer 0°		**Layer 90°**		**Layer 0°**		**Fibre**	**Matrix**
$Energy_{Total}$	1.0885		0.6101		0.7590		0.1025	0.2273
$Energy_{Inplanep}$	0.8456		0.0459		0.5292		0.0959	0.1960
$Energy_{Outplane}$	0.2429		0.5654		0.2298		0.0066	0.0313

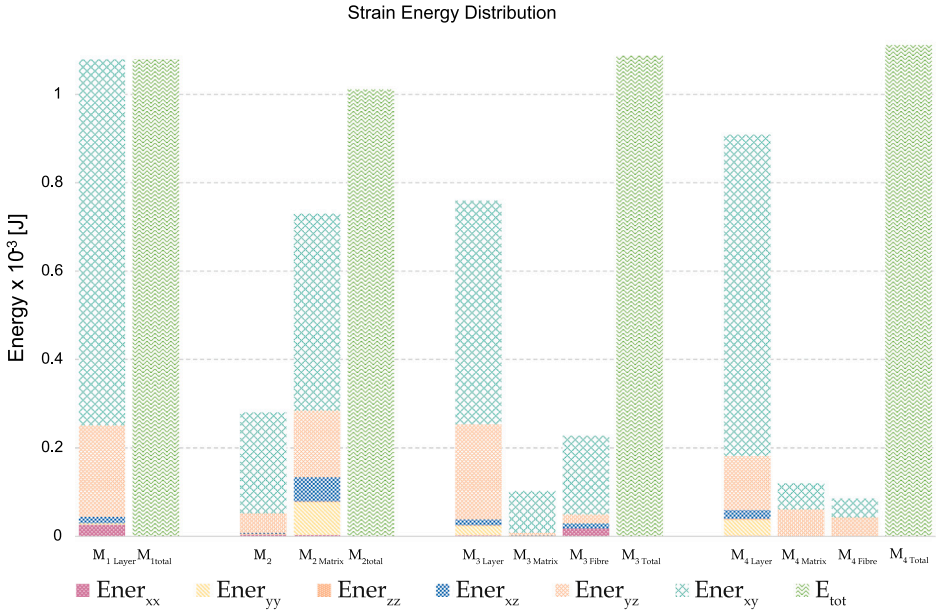

Fig. 20. The contributions of strain energy due to the six stress components, evaluated for the proposed models.

Table 8
Strain energy distribution evaluated in each component for Model 2 in bending and twisting load case.

	Energy Distribution Single Component							
	Model 2 x 10 $^{-3}$ [J] - Bending							
	Fibre 1	**Fibre 2**	**Fibre 3**	**Fibre 4**	**Fibre 5**	**Fibre 6**	**Fibre 7**	**Fibre 8**
$Ener_{xx}$	3.1E−05	0.00022	0.00022	3.1E−05	3.3E−05	0.00022	0.00022	−3.1E−05
$Ener_{yy}$	0.948225	0.948375	0.948375	0.948225	0.879244	0.948375	0.948375	0.948225
$Ener_{zz}$	9.46E−05	0.000192	0.000192	9.46E−05	9.34E−05	0.000192	0.000192	9.46E−05
$Ener_{xz}$	2.2E−05	6.19E−06	6.19E−06	2.2E−05	3.97E−05	6.19E−06	6.19E−06	2.2E−05
$Ener_{yz}$	5.92E−05	6.33E−05	6.33E−05	5.92E−05	0.00022	6.33E−05	6.33E−05	5.92E−05
$Ener_{xy}$	2.27E−05	3.1E−06	3.1E−06	2.27E−05	2.08E−05	3.1E−06	3.1E−06	2.27E−05
	Matrix 1	**Matrix 2**	**Matrix 3**	**Matrix 4**	**Matrix 5**	**Matrix 6**	**Matrix 7**	**Matrix 8**
$Ener_{xx}$	0.017401	0.017401	0.00049	0.00049	0.00014	0.00014	7.16E−05	7.16E−05
$Ener_{yy}$	0.017204	0.017204	0.00033	0.00033	0.00019	0.00019	0.000134	0.000134
$Ener_{zz}$	0.017401	0.017401	0.00049	0.00049	0.00014	0.00014	7.16E−05	7.16E−05
$Ener_{xz}$	0.017204	0.017204	0.00033	0.00033	0.00019	0.00019	0.000134	0.000134
$Ener_{yz}$	0.017204	0.017204	0.00033	0.00033	0.00019	0.00019	0.000134	0.000134
$Ener_{xy}$	0.017401	0.017401	0.00049	0.00049	0.00014	0.00014	7.16E−05	7.16E−05
	Model 2 x 10 $^{-3}$ [J] - Twisting							
	Fibre 1	**Fibre 2**	**Fibre 3**	**Fibre 4**	**Fibre 5**	**Fibre 6**	**Fibre 7**	**Fibre 8**
$Ener_{xx}$	3.45E−05	0.000869	0.000869	3.45E−05	3.41E−05	0.000869	0.000869	3.45E−05
$Ener_{yy}$	0.00117	0.00039	0.00039	0.00117	0.001135	0.00039	0.00039	0.00117
$Ener_{zz}$	1.53E−05	0.000386	0.000386	1.53E−05	1.53E−05	0.000386	0.000386	1.53E−05
$Ener_{xz}$	2.89E−05	0.001018	0.001018	2.89E−05	3.05E−05	0.001018	0.001018	2.89E−05
$Ener_{yz}$	0.007483	0.003523	0.003523	0.007483	0.02908	0.003523	0.003523	0.007483
$Ener_{xy}$	0.037215	0.078315	0.078315	0.037215	0.035532	0.078315	0.078315	0.037215
	Matrix 1	**Matrix 2**	**Matrix 3**	**Matrix 4**	**Matrix 5**	**Matrix 6**	**Matrix 7**	**Matrix 8**
$Ener_{xx}$	0.00003	0.00021	0.00021	0.00003	0.00003	0.00031	0.00021	0.00003
$Ener_{yy}$	0.00017	0.02665	0.02665	0.00017	0.00017	0.04551	0.02665	0.00017
$Ener_{zz}$	0.00004	0.00003	0.00003	0.00004	0.00004	0.00005	0.00003	0.00004
$Ener_{xz}$	0.00016	0.01835	0.01835	0.00016	0.00016	0.03367	0.01835	0.00016
$Ener_{yz}$	0.06124	0.01322	0.01322	0.06124	0.06124	0.01318	0.01322	0.06124
$Ener_{xy}$	0.06335	0.15093	0.15093	0.06335	0.06335	0.16594	0.15093	0.06335

Finally, in Fig. 20, the contributions of strain energy calculated as integral quantities over the elements constituting the various components are highlighted, in the case of torsional loading. Fig. 20 presents the strain energy values for the lower layer of models LW, CM, and LW-CW (the second configuration with a single fibre, previously described, is identified by the number 4, while for all configurations, the letter M in the figure refers to the Model). It is evident that out-of-plane contributions are absorbed by the matrix; however, an LW-type model, unlike a CW model, does not allow for an accurate evaluation of the energy contributions absorbed by the various components. Furthermore, even the LW-CW model is influenced by the choice of fibre position.

4. Conclusions

This paper offers a comprehensive exploration of strain energy absorption in fibre-reinforced composite structures using different model scales. The Component-Wise (CW) formulation, derived from the 1D Carrera Unified Formulation (CUF) structural models, provides a framework capable of individually modeling laminates, laminae, fibres, and matrices. This unique capability enables the modeling of components at different scales within the same 1D formulation. The results obtained with the CW approach show a remarkable alignment with those from solid models, demonstrating high accuracy while significantly reducing computational costs. Three models were developed for macro-, meso-, and micro-scale analysis of the problem, with degrees of freedom (DOFs) of 5445, 22,869, and 59,169, respectively, compared to the reference solid model, which utilizes 4,932,459 DOFs. Notably, Model 3 achieves the same in-plane and out-of-plane stress distribution as the commercial solid element model, using only 12% of its DOFs.

The comprehensive analysis of strain energy across each stress–strain component direction serves as a powerful tool for qualitatively identifying regions that are more prone to absorbing large amounts of energy and potentially initiating failure phenomena within composite structures. However, to fully leverage this approach, careful attention must be given to the selection of sub-volume distributions. Specifically, prioritizing distributions that encompass individual components within the cross-section yields optimal results. This strategic choice enables a precise evaluation of local effects. By focusing on sub-volume distributions that isolate single components, such as fibres or matrices, researchers can effectively capture localized variations in strain energy and stress concentrations. The future works will focus on the analysis of more complex composite material structures, eventually using plate and shell models. These models will allow for a deeper understanding of the structural behavior under various loading conditions, providing a more comprehensive evaluation of composite materials in advanced applications.

CRediT authorship contribution statement

R. Augello: Writing – review & editing, Supervision, Methodology, Investigation, Data curation, Conceptualization. **E. Carrera:** Writing – review & editing, Validation, Supervision, Software, Resources, Methodology, Data curation, Conceptualization. **S. Saputo:** Writing – review & editing, Writing – original draft, Methodology, Investigation, Formal analysis, Data curation, Conceptualization.

Declaration of competing interest

The authors declare that they have no known competing financial interests or personal relationships that could have appeared to influence the work reported in this paper.

Acknowledgements

This work is part of the project NOVITAS, funded by the European Union's Horizon Europe research and innovation program under the Marie Sklodowska-Curie grant agreement No 101059825.

Data availability

No data was used for the research described in the article.

References

[1] Begley JA, Landes JD. The fracture toughness: Part II. ASTM International; p. 1–1–23.

[2] Pinho ST, Robinson P, Iannucci L. Fracture toughness of the tensile and compressive fibre failure modes in laminated composites. Compos Sci Technol 2006;66(13):2069–79.

[3] Carrera Erasmo. Evaluation of layerwise mixed theories for laminated plates analysis. AIAA J 1998;36(5):830–9.

[4] Robbins DH, Reddy JN. Modelling of thick composites using a layerwise laminate theory. Internat J Numer Methods Engrg 1993;36(4):655–77.

[5] Carrera E, Giunta G. Refined beam theories based on Carrera's unified formulation. Int J Appl Mech 2010;2(1):117–43.

[6] Pandya B, Kant T. Higher-order shear deformable theories for flexure of sandwich plates. Finite element evaluations. Int J Solids Struct 1988;24(12):1267–86.

[7] Reddy JN. A simple higher-order theory for laminated composites. J Appl Mech 1986;51:745–52.

[8] Ferreira A, Roque C, Jorge R. Analysis of composite plates by trigonometric shear deformation theoryand multiquadrics. Comput Struct 2005;83(27):2225–37.

[9] Ren S, Cheng C, Meng Z, Zhao G. A new general third-order zigzag model for asymmetric and symmetric laminated composite beams. Compos Struct 2021;260(16).

[10] Reissner E. On a mixed variational theorem and on shear deformable plate theory. Internat J Numer Methods Engrg 1986;23(2):193–8.

[11] Kapania Rakesh K, Raciti Stefano. Recent advances in analysis of laminated beams and plates, Part II: Vibrations and wave propagation. AIAA J 1989;27(7):935–46.

[12] Pagano N. Exact solutions for composite laminates in cylindrical bending. J Compos Mater 1969;3(3):398–411.

[13] Pineda E, A. Waas. Multiscale failure analysis of laminated composite panels subjected to blast loading using feamac/explicit. NASA/ TM, 2009, p. 215–813.

[14] Sun C, Vaidya R. Prediction of composite properties from a representative volume element. Compos Sci Technol 1996;56(2):171–9.

[15] Yu W. A unified theory for constitutive modeling of composites. J Mech Mater Struct 2016;11(4):379–411.

[16] Maiarú M, Petrolo M, Carrera E. Evaluation of energy and failure parameters in composite structures via a Component-Wise approach. Composites B 2017;108:53–64.

[17] E. Carrera, M. M Cinefra, M. Petrolo, E. Zappino. Finite element analysis of structures through unified formulation. Hoboken, USA: John Wiley Sons; 2014.

[18] Pagani A, Petrolo M, Carrera E, Colonna G. Ynamic response of aerospace structures by means of refined beam theories. Aerosp Sci Technol 2015;46:360–73.

[19] Carrera E, Pagani A, Petrolo M. Component-wise method applied to vibration of wing structures. J Appl Mech 2013;80(4).

[20] Carrera E, Pagani A. Free vibration analysis of civil engineering structures by component-wise models. J Sound Vib 2014;333(19).

[21] Carrera E, Maiarú M, Petrolo M. Component-wise analysis of laminated anisotropic composites. Int J Solids Struct 2012;49(13):1839–51.

[22] Carrera Erasmo, Maiaru Marianna, Petrolo Marco. Evaluation of failure parameters in composite structures by component-wise approach. In: 54th AIAA/ASME/ASCE/AHS/ASC structures, structural dynamics, and materials conference. American Institute of Aeronautics and Astronautics; 2013.

[23] Reddy JN. Mechanics of laminated composite plates and shells. Theory and analysis. 2nd ed. CRC Press; 2004.

[24] Bathe KJ. Finite element procedure. Upper Saddle River, New Jersey, USA: Prentice Hall; 1996.

[25] Cinefra M, D'Ottavio M, Polit O, Carrera E. Assessment of MITC plate elements based on CUF with respect to distorted meshes. Compos Struct 2020;238:111962.

[26] Cinefra M, Valvano S. A variable kinematic doubly-curved MITC9 shell element for the analysis of laminated composites. Mech Adv Mater Struct 2016;23(11):1312–25.

[27] Carrera E, de Miguel AG, Pagani A. Micro-, meso- and macro-scale analysis of composite laminates by unified theory of structures. 2017.

[28] Pagani A, Carrera E, Augello R, Scano D. Use of Lagrange polynomials to build refined theories for laminated beams, plates and shells. Compos Struct 2021;276:114505.